Journal of The Electrochemical Society

OPEN ACCESS

Lithium Insertion in Nanostructured $Si_{1-x}Ti_x$ Alloys

Lithium Insertion in Nanostructured $Si_{1-x}Ti_x$ Alloys

Yukun Wang,[a,b] Simeng Cao,[a] Mariya Kalinina,[a] Lituo Zheng,[a] Linjun Li,[a] Min Zhu,[b] and M. N. Obrovac[a,c,z]

[a]*Department of Chemistry, Dalhousie University, Halifax, N.S., B3H 4R2, Canada*
[b]*School of Materials Science and Engineering and Key Laboratory of Advanced Energy Storage Materials of Guangdong Province, South China University of Technology, Guangzhou 510641, People's Republic of China*
[c]*Department of Physics and Atmospheric Science, Dalhousie University, Halifax, N.S., B3H 4R2 Canada*

Nanostructured $Si_{1-x}Ti_x$ alloys ($0 \leq x \leq 0.3$) prepared by ball milling were studied as negative electrode materials in Li cells. The alloys comprised a nanocrystalline and amorphous Si phase and a nanocrystalline C49 $TiSi_2$ phase. When $x \geq 0.15$ the nanocrystalline Si phase was completely eliminated and such alloys consisted only of amorphous Si and the C49 $TiSi_2$ phase. The alloys with $x \geq 0.15$ also completely suppressed the formation of $Li_{15}Si_4$ during cycling, resulting in good capacity retention, and, unlike other Si transition metal alloys, without introducing noticeable cell polarization. The observed capacity of the $Si_{1-x}Ti_x$ alloys suggested that the $TiSi_2$ is an inactive phase toward Li. The $Si_{0.85}Ti_{0.15}$ composition had a high capacity of 1710 Ah/L with 96% capacity retention after 50 cycles, making it attractive for use in Li-ion batteries.

Manuscript submitted July 5, 2017; revised manuscript received September 18, 2017. Published September 30, 2017.

Silicon-based materials are of high interest in the pursuit of obtaining higher energy density lithium ion batteries. Pure silicon has an outstanding theoretical capacity of 2194 Ah/L, which has been estimated to provide an increase in energy density of up to 34% in Li-ion cells, compared to cells with conventional graphite-based electrodes.[1] However, the cycle life of Si electrodes is difficult to maintain because of its drastic volume expansion during lithiation (up to 280%). Reducing Li uptake and providing an inactive phase framework is one possible way to alleviate the expansion problem. Some inactive M-Si alloys, such as Ni-Si,[2–4] Fe-Si,[5] Cu-Si,[6] B-Si,[7] have been extensively studied in the past two decades.

Si-Ti alloys are of interest as electrode materials for Li-ion batteries because of their thermal stability and because they are composed of high abundance elements. They also have low density and $TiSi_2$ has high electrical conductivity compared to other silicides.[8] Because of these favorable properties, this system has been studied by other groups in the past. Lee et al. synthesized Si-Ti alloys via melt spinning, forming alloys comprised of well crystallized Si and $TiSi_2$ phases.[9] The observed capacities of these samples in Li cells were far less than expected from the amount of Si present. All the Si in these samples might not have been fully accessible to lithium ions because of the morphology that resulted from rapid solidification processing. Zhou et al. synthesized Si coated $TiSi_2$ nanonets via chemical vapor deposition.[10] When the nanonets were cycled between 0.03–3.0 V, high capacity fade during cycling resulted because of the formation of $Li_{15}Si_4$. When cycling was conducted above 0.09 V, capacity retention was improved because the formation of $Li_{15}Si_4$ was avoided. This indicates the importance of avoiding $Li_{15}Si_4$ formation to obtain good cycling performance. Park et al. designed a $TiSi_2$-coated Si anode via a silicothermic reduction process.[11] The conductive silicide coating resulted in improved rate performance. It is apparent from these studies that microstructure and $Li_{15}Si_4$ avoidance is important in obtaining good cycling in Si-Ti alloys. However, to our knowledge a systematic study of the effect of composition in the Si-Ti alloy system has not previously been reported.

Here a careful study of $Si_{1-x}Ti_x$ alloys produced by mechanical milling is presented. An optimized milling technique[12] was used to obtain materials with a highly amorphous/nanocrystalline microstructure. The resulting alloys comprise amorphous Si and a metastable nanocrystalline $TiSi_2$ C49 phase that has a large number of crystal defects. Electrochemical studies indicate the relationship between the microstructure, $Li_{15}Si_4$ formation and cycling performance. Some of the $Si_{1-x}Ti_x$ alloys were found to have high reversible capacity with excellent capacity retention.

Experimental

$Si_{1-x}Ti_x$ (where $0 \leq x \leq 0.3$, $\Delta x = 0.05$) alloys were prepared by ball milling Ti (Alfa, −325 mesh, 99% metals basis) and silicon (Aldrich, −325 mesh, 99% metals basis) powders. A 0.5 mL total reactant powder volume together with 180 g 1/16-inch stainless steel balls were loaded into milling vials and sealed under argon atmosphere. The samples were ball milled in a SPEX 8000D dual mixer mill under conditions optimized to result in amorphous alloys, as we describe in a previous study.[12] These milling conditions typically result in about 1 atomic % Fe contamination.[12]

X-ray diffraction (XRD) patterns were collected using a Rigaku Ultima IV diffractometer equipped with a Cu Kα X-ray source and a diffracted beam monochromator. Each XRD scan was collected from 20° to 60° 2-theta in 0.05° increments for 3 seconds per step. True sample densities were measured using a Micromeritics AccuPyc II 1340 gas pycnometer. Oxygen content was determined by LECO testing (NSL Analytical Services, Inc, Cleveland OH). Scanning electron microscope (SEM) images were measured using a TESCAN MIRA 3 field-emission scanning electron microscope.

All alloys made were found to be water stable. Electrode slurries were made by mixing $Si_{1-x}Ti_x$ alloys, carbon black (Super C65, Imerys Graphite & Carbon) and a 10 weight% aqueous solution of lithium polyacrylate (LiPAA), made by neutralizing a polyacrylic acid solution (Sigma-Aldrich, average molecular weight∼250,000 g/mole, 35 wt% in H_2O) with $LiOH \cdot H_2O$ (Sigma Aldrich, 98%) in distilled water) with a volumetric ratio of 70/5/25 (80±4/5/15 by weight) in distilled water. The mixing was conducted in a planetary ball mill (Retsch PM200) with 3 WC balls (15:1 ball/sample weight ratio) at 100 rpm for a period of 1 h. The slurries were coated on electrolytic Cu foil (Furukawa Electric, Japan) using a 0.004-inch gap coating bar and dried at 120°C in air for 1 h. Typical electrode loadings were about 3.0 mAh/cm^2.

Electrodes were assembled in 2325-type coin cells with a lithium foil counter/reference electrode. Two layers of Celgard 2300 separator were used in each coin cell. 1 M $LiPF_6$ (BASF) in a solution of ethylene carbonate, diethyl carbonate and monofluoroethylene carbonate (volume ratio 3:6:1, all from BASF) was used as electrolyte. Cell assembly was carried out in an Ar-filled glove box. Cells were cycled galvanostatically at 30.0 ± 0.1°C between 0.005 V and 0.9 V using a Maccor Series 4000 Automated Test System at a C/10 rate for the

[z]E-mail: mnobrovac@dal.ca

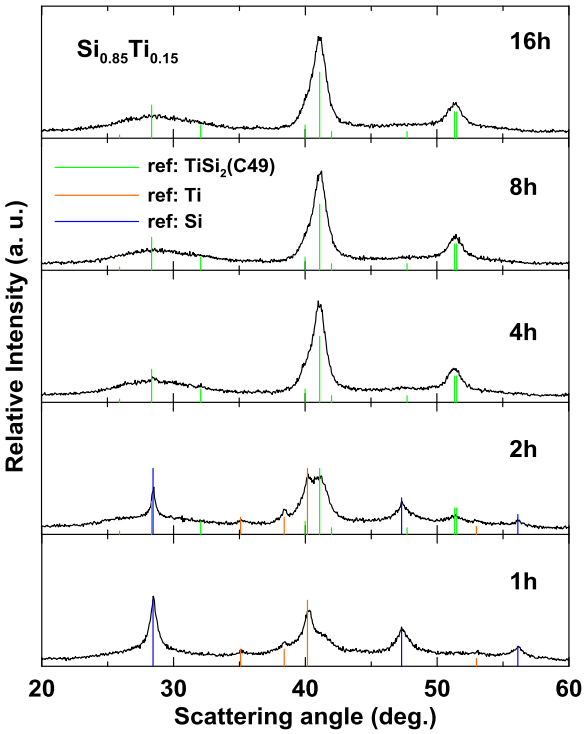

Figure 1. X-ray diffraction patterns of $Si_{0.85}Ti_{0.15}$ prepared using different milling times.

first two cycles and a C/5 rate for the following cycles with a C/20 trickle discharge (lithiation). After cycling, the cells were stopped at a potential of 3.0 V and then disassembled in an Ar-filled glove box. Harvested negative electrodes were then washed with dimethyl carbonate (BASF) to remove residual electrolyte and dried under vacuum. These electrodes were then transferred to the SEM for imaging without air exposure, using gastight sample transfer containers.

Results and Discussion

XRD patterns of the $Si_{0.85}Ti_{0.15}$ alloys prepared by ball milling for 1–16 h are shown in Figure 1. After 1 h milling, the sample comprises peaks from nanocrystalline Si and Ti phases, indicating the milling was incomplete. With increased milling time, the nanocrystalline Si and Ti peak intensities decline, the Si peak near 28° is replaced with a very broad peak corresponding to amorphous Si, and two new broad peaks located at 41° and 53° rise progressively. After 8 h, the reaction becomes complete, as no reactant peaks remain, and reaches a steady-state, as the peaks of the resultant products do not change or broaden with longer milling time. The peaks at 41° and 53° correspond to those from the metastable orthorhombic C49 $TiSi_2$ phase, which has been synthesized previously by ball milling by Yan et al.[13] However, two low angle peaks reported for the C49 phase at about 28° and 32° corresponding to the (021) and (130) lattice planes, respectively, are missing in our XRD patterns. Interestingly, these peaks were also absent in samples prepared by Yan et al., who suggested that the "absence of these lines may be explained by chemical disorder of the structure induced by milling, causing superlattice lines to disappear." We have not found any reports of a C49 $TiSi_2$ phase where these peaks have actually been observed.

To study the C49 phase more carefully, a $Si_{0.67}Ti_{0.33}$ alloy was prepared by ball milling and annealed at 600°C for 12 h to obtain a C49 $TiSi_2$ sample having good crystallinity. The XRD pattern of this sample is shown in Figure 2. Despite the improved crystallinity of the sample, peaks near 28° and 32° were still not observed, with only a broad feature being present in this vicinity. Rietveld refinement of this XRD pattern resulted in good refinements when significant site vacancies

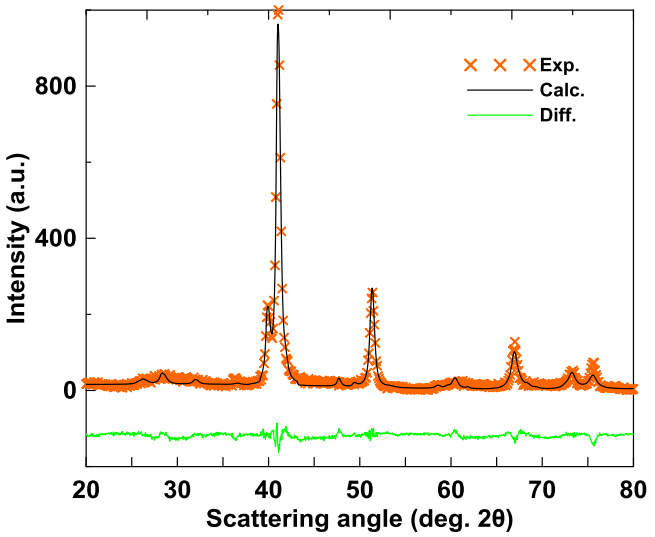

Figure 2. X-ray diffraction pattern and Rietveld refinement result of $Si_{0.67}Ti_{0.33}$.

were introduced, as shown in Figure 2 and Table I. The vacancy concentration corresponds to a composition of $Ti_{0.74}\square_{0.26}(Si_{0.92}\square_{0.08})_2$. This high vacancy concentration may have been induced by plastic deformation during ball milling and is consistent with the explanation of Yan et al. for the missing (021) and (130) lattice reflections.

A series of $Si_{1-x}Ti_x$ samples (where $0 \leq x \leq 0.3$, $\Delta x = 0.05$) were prepared for further investigation. All samples were milled for the 8 h milling time that was shown to achieve reaction completion and steady-state microstructure for the $Si_{0.85}Ti_{0.15}$ composition discussed above. LECO testing revealed that the Si precursor comprised a significant oxygen impurity of about 8 atomic % (presumably present as an oxide in the Si powder as received). Therefore these alloys contain at least 8 atomic % oxygen with respect to their Si content. The XRD patterns of these samples are shown in Figure 3. The XRD pattern of the $x = 0$ sample (pure Si) has peaks which appear to be composed of a nanocrystalline Si component and an amorphous Si component. When the Ti content is increased, the intensity of the nanocrystalline Si (111) peak at 28.4° progressively reduces. When $x \geq 0.15$, the nanocrystalline Si component is no longer present and only a broad feature corresponding to amorphous Si could be observed near the Si (111) peak position. Meanwhile, peaks relating to the C49 $TiSi_2$ phase grow with increasing Ti content. From these observations, it can be concluded that the reduction of nanocrystalline Si content is coincidental with the presence of the C49 phase. This might be because the presence of the C49 phase limits the Si domain size, preventing its aggregation and recrystallization during the milling process. It's also noticeable that a small broad feature near 38° appears in the XRD patterns of many of the samples, especially $Si_{0.95}Ti_{0.05}$. The only peak we could ascribe this feature to was the (002) Ti peak from residual Ti being present in the samples. However, even when the milling time was extended to 32 h, this peak still remained. We suspect this

Table I. Parameters used for Rietveld refinement of C49 $TiSi_2$. Using space group Cmcm (No. 63).

atom	site	x	y	z	occupancy
Ti	4c	0	0.414(6)	1/4	0.742(8)
Si	4c	0	0.059(0)	1/4	0.845(3)
Si	4c	0	3/4	1/4	1

a = 3.561(2) Å, b = 13.53(5) Å, c = 3.549(5) Å, R_b = 4.86%, and R_{wp} = 25.046%.

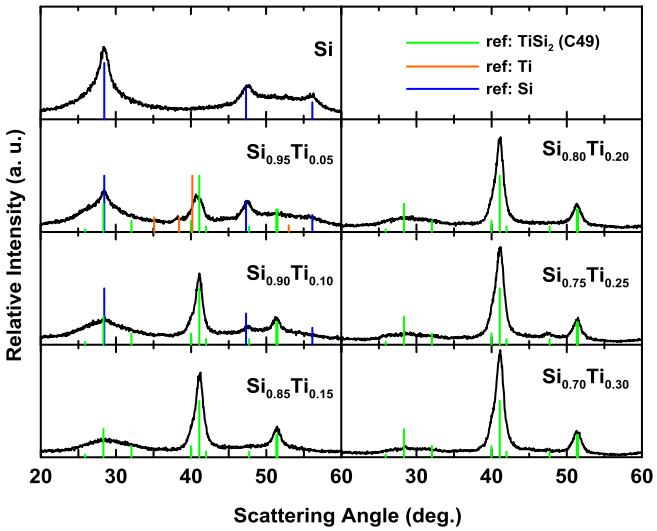

Figure 3. XRD patterns of ball milled $Si_{1-x}Ti_x$ alloys ($0 \leq x \leq 0.3$).

peak may represent Ti that was adhered to a dead-space (e.g. corners) within the milling vessel. Since the relative area under this peak is small, it should have little effect on the alloy stoichiometry and electrochemistry.

The electrochemical performance of $Si_{1-x}Ti_x$ alloys was investigated by galvanostatic cycling in Li cells. Figures 4a–4g shows the voltage profiles of the $Si_{1-x}Ti_x$ alloys. Corresponding differential capacity curves are shown in Figures 5a–5g. Upon initial lithiation a sharp peak is present in most of the differential capacity curves. This peak often arises during the first lithiation of alloys and is attributed to the initial nucleation and growth of Li-alloys during the first lithium insertion process.[1] In Figure 4a the voltage curve of ball milled Si comprises two sloping plateaus characteristic of amorphous Si during the first lithiation,[14] followed by a flat voltage plateau at 0.45 V during delithiation and a corresponding peak in the differential capacity (Figure 5a). This peak is characteristic of $Li_{15}Si_4$ formation when Si electrodes are discharged to a voltage below 50 mV.[14] The size of the 0.45 V peak progressively decreases with the increasing x, suggesting a suppression of $Li_{15}Si_4$ phase with the introduction of $TiSi_2$. At a composition of $Si_{0.85}Ti_{0.15}$ the 0.45 V peak is no longer present, and the differential capacity is characteristic of the cycling of amorphous Li-Si in a single-phase region,[14] as shown in Figure 4d and Figure 5d. The suppression of $Li_{15}Si_4$ phase formation is maintained during all of the 50 charge/discharge cycles tested. $Li_{15}Si_4$ phase suppression is also achieved in the Ni-Si alloy system, due to a stress-potential coupling effect.[3] Fe-Si[5] and Cu-Si[6] alloys also exhibit lithiation voltage depression and increased polarization with increasing transition metal content. Uniquely, no significant change in average discharge or charge voltage is observed in $Si_{1-x}Ti_x$ alloys. Therefore, the mechanism by which $Li_{15}Si_4$ phase formation is suppressed in this alloy system may be different and results in $Li_{15}Si_4$ suppression accompanied by no noticeable increase in cell polarization, in contrast to Si-Ni,[3] Si-Fe[5] and Si-Cu[6] alloys. Interestingly, $Li_{15}Si_4$ suppression is coincident with the disappearance of the nanocrystalline Si phase observed in the XRD patterns, as discussed above, indicating that the Si microstructure may have substantial influence on $Li_{15}Si_4$ suppression.

All of the voltage curves shift toward higher specific capacities as cycling progresses. This slippage effect is due to reactions with the electrolyte that contribute to SEI formation and/or the formation of soluble electrolyte decomposition products.[15] All such reactions involve the consumption of Li, which leads to poor coulombic efficiency and cell fade in full cells. The reactivity with electrolyte is most severe for pure Si, where the voltage curve slippage is greatest. The amount of slippage reduces with increasing Ti content and only reduces to zero as the capacity also approaches zero. This suggests

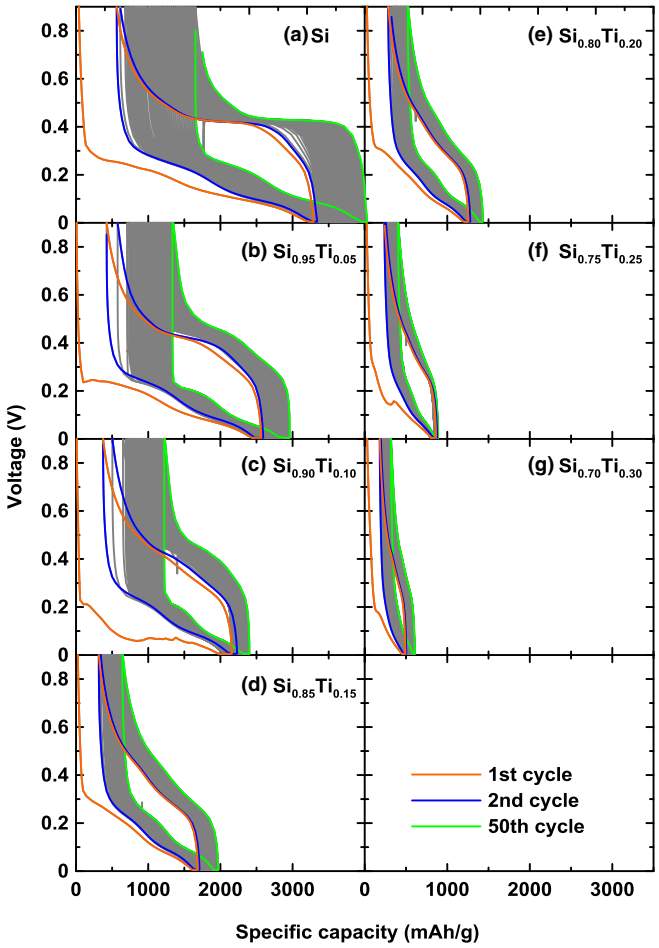

Figure 4. Voltage curves of $Si_{1-x}Ti_x$ alloy electrodes cycled between 0.005 V and 0.9 V.

that the reactivity with electrolyte is related directly to the relative volume expansion of each alloy, which has been suggested previously also.

The specific capacity of $Si_{1-x}Ti_x$ alloys versus cycle number is shown in Figure 6. Significant capacity fade is observed for alloys with high Si content ($x < 0.15$). This fade rate is not related to volume expansion, since the fade rate is the same regardless of alloy composition or capacity in the composition range. At a composition of $Si_{0.85}Ti_{0.15}$, the fade rate suddenly becomes nearly zero for the 50 cycles tested. This is also the composition at which $Li_{15}Si_4$ formation is suppressed. Therefore, we suspect that the fade observed for high Si contents is related to cycling in the 2-phase region formed when $Li_{15}Si_4$ is present.

To investigate the fade mechanism, the microstructure of uncycled electrodes and electrodes cycled 50 times was inspected by SEM. Figures 7a and 7c respectively show the surface of uncycled Si and $Si_{0.85}Ti_{0.15}$ electrodes. Both uncycled electrode coatings are dense and smooth, excepting that a similar crack pattern is present in both. This crack pattern occurs because the PAA binder shrinks during the drying process. Figures 7b and 7d respectively show the surface of Si and $Si_{0.85}Ti_{0.15}$ electrodes that have been cycled 50 times. After cycling, the Si electrode adhesion to the current collector was extremely poor and the entire coating lost its structural integrity. Despite careful handling, only a fraction of the electrode coating remained on the current collector for SEM analysis. The high volume expansion of pure Si during lithiation and internal fracturing of the Si particles themselves from the a-Li_xSi/$Li_{15}Si_4$ 2-phase region during delithiation are likely to both have contributed to the loss of structural integrity. As a result, it seems that the only means of providing electrical contact within the

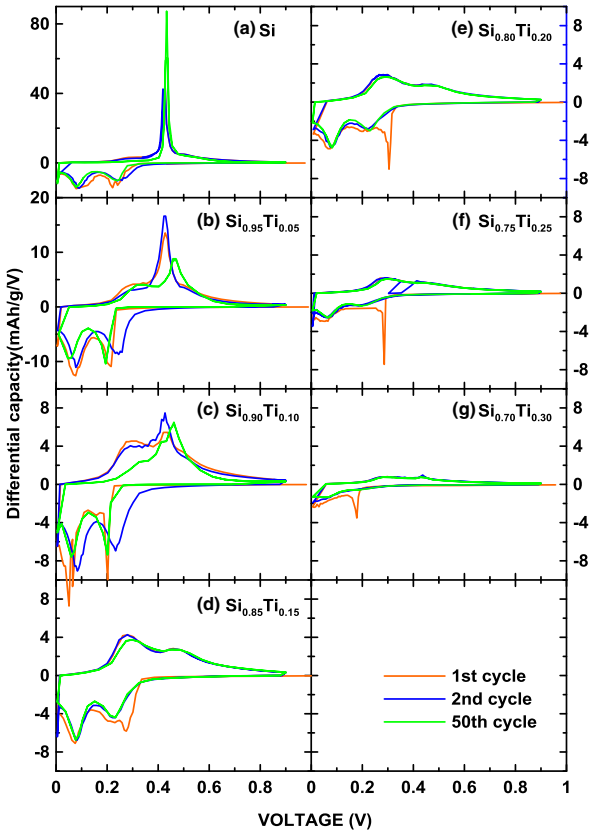

Figure 5. Differential capacity curves of $Si_{1-x}Ti_x$ alloy electrodes derived from Figure 4 for the 1st (blue) and 2nd (red) cycles.

coating was from the cell stack pressure. Nevertheless, many particles became electrically disconnected, as evidenced by the large capacity fade for this composition.

In contrast, the cycled $Si_{0.85}Ti_{0.15}$ electrode shown in Figure 7d shows much better structural integrity. The charge/discharge cycling only resulted in a slight change in the crack pattern on the electrode surface. That is, the cracks became wider and the crack density increased. The well-maintained electrode structural integrity is reflected in the good cycling performance of this electrode, in which almost no capacity fade was observed during 50 cycles. It is likely that the increased structural integrity of this electrode arises from the reduced volume expansion of $Si_{0.85}Ti_{0.15}$ during lithiation (~135%) compared to that of Si (280%) and from the avoidance of the a-Li_xSi/$Li_{15}Si_4$ 2-phase region. It is also possible that the addition of Ti may have improved adhesion to the binder also, but this effect requires further study.

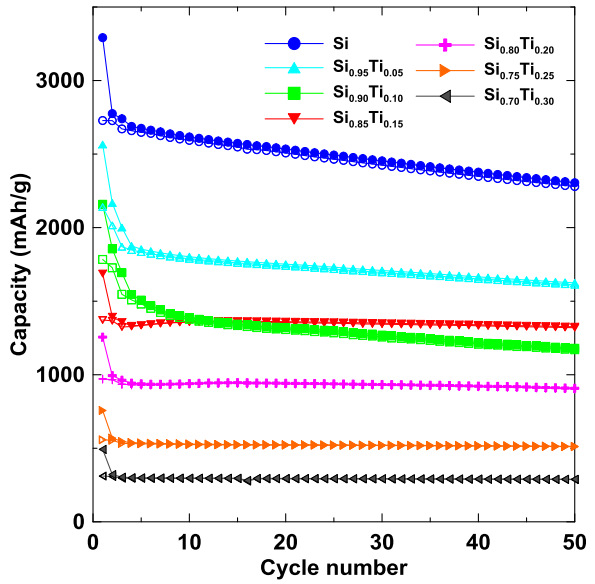

Figure 6. Lithiation (closed symbols) and delithiation (open symbols) capacity of ball milled $Si_{1-x}Ti_x$ alloys versus cycle number.

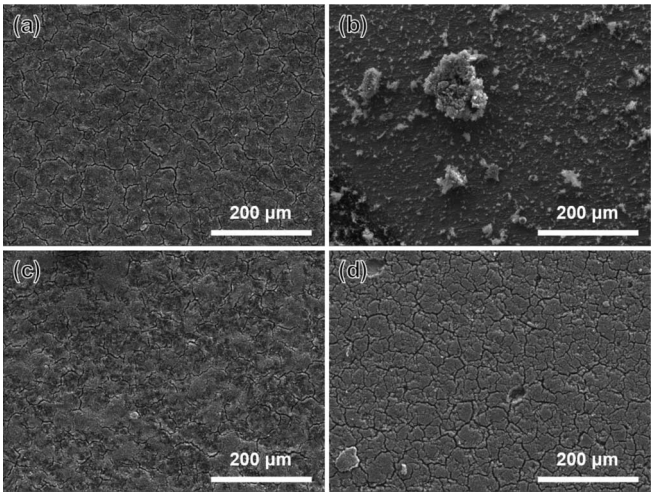

Figure 7. SEM images of Si (a, b) and $Si_{0.85}Ti_{0.15}$ (c, d) electrodes. (a) and (c) are electrodes as prepared, (b) and (d) are electrodes after 50 charge/discharge cycles.

The $Si_{0.85}Ti_{0.15}$ phase has a reversible capacity of 1372 mAh/g or 1750 Ah/L with an initial coulombic efficiency of 81%. Reversible capacities then decrease as Ti is added to the alloy, as expected. Figure 8 shows the first lithiation and delithiation capacities of $Si_{1-x}Ti_x$ alloys as a function of x. Typically first lithiation capacities represent the full alloy capacity plus any irreversible capacity associated with irreversible side reactions, including solid electrolyte interphase formation. The first delithiation capacity typically represents a capacity that is less than the alloy capacity, due to alloy fracture disconnection as the alloy particles contract. As volume expansion becomes less, the amount of capacity lost due to this effect is expected to decrease. Also shown in Figure 7 is a curve representing the theoretical capacity

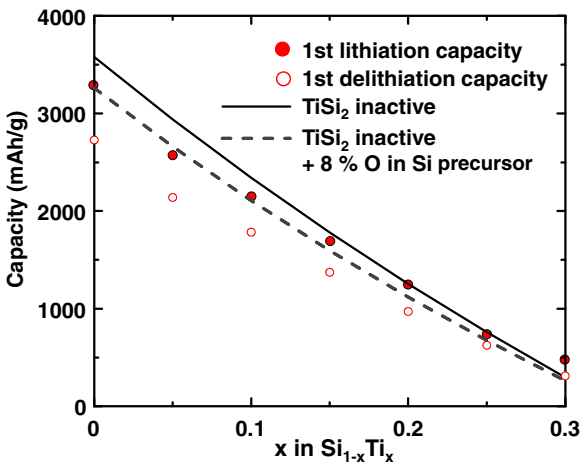

Figure 8. The first lithiation (closed circles) and delithiation (open circles) capacities of $Si_{1-x}Ti_x$ alloys. Also shown are theoretical capacity calculations assuming that the $TiSi_2$ phase is inactive (solid curve) and that additionally an 8 atomic % oxygen content in the Si precursor forms inactive SiO_2.

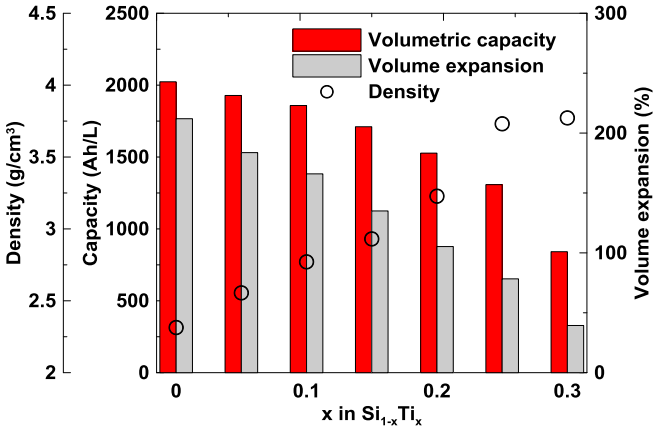

Figure 9. Density, volumetric capacity, volume expansion at full lithiation of ball milled $Si_{1-x}Ti_x$ alloys versus x.

assuming that all of the Ti in the alloy reacts with Si to form $TiSi_2$ as an electrochemically inactive phase. This theoretical capacity is larger than the first lithiation capacity, which does not make physical sense, since the measured first lithiation capacity should be larger than the theoretical capacity as discussed above. A probable reason for the low measured capacity is the 8 atomic % oxygen content in the Si precursor, which would tend to react with the Si to form inactive SiO_2. The dashed line in Figure 7 takes into account this effect, resulting in a theoretical capacity model that lies roughly between the first lithiation capacities and first delithiation capacities, as expected. Although this simple model fits the capacity well and is consistent with the XRD phase analysis, the situation may be more complicated than the model suggests. For instance, the highly nonstoichiometric nature of the $TiSi_2$ phase, suggested from Rietveld refinement, suggests that each Ti atom might be able to inactivate more than 2 Si atoms, which would lower the capacity. Regardless of this, it is abundantly clear that any $TiSi_2$ phases formed are electrochemically inactive.

The volumetric capacity and volume expansion (as determined theoretically from the measured density and reversible capacity[1]) of $Si_{1-x}Ti_x$ alloys is shown in Figure 9. Both of them decrease accordingly with increasing Ti content. However, the relative decrease of the volumetric capacity is less severe than the gravimetric capacity, since the alloy density (also shown in Figure 9) increases with Ti content. Of these alloys, the $Si_{0.85}Ti_{0.15}$ composition is the alloy having highest volumetric capacity while not exhibiting $Li_{15}Si_4$ formation during cycling and retaining good capacity retention. This alloy has a volumetric capacity of 1710 Ah/L, which is over double that of graphite. This combined with the high abundance of its constituents and high specific capacity (2751 mAh/g), make this material and others in the Si-Ti alloy series attractive for use in negative electrodes in Li-ion batteries.

Conclusions

A systematic study of ball-milled Si-Ti alloys was conducted. These alloys were found to comprise amorphous/nanocrystalline Si phases and a nanocrystalline $TiSi_2$ C49 phase with a high defect concentration. The $TiSi_2$ phase was found to be electrochemically inactive, but effectively suppressed the formation of $Li_{15}Si_4$ during cycling when the Ti content was 85 atomic % or greater. At this composition the nanocrystalline Si phase was eliminated and only amorphous Si remained in the alloy. The $Li_{15}Si_4$ phase suppression was achieved at a high volumetric capacity (1710 Ah/L) and with no noticeable change in the alloy average voltage (in contrast to Si-Ni, Cu, and Fe alloys), resulting in relatively low polarization cycling. The $Li_{15}Si_4$ phase suppression was also coincident with good cycling performance and with good electrode structural integrity. These characteristics of Si-Ti alloys as well as the high atomic abundance of their constituents make them attractive for use in negative electrodes in Li-ion batteries.

Acknowledgment

The authors acknowledge funding from NSERC and 3M Canada, Co. under the auspices of the Industrial Research Chair and Discovery grant programs. Yukun Wang acknowledges financial support from the SCUT Doctoral Student Short-Term Overseas Visiting Study Funding Project.

References

1. M. N. Obrovac and V. L. Chevrier, *Chem. Rev.*, **114**, 11444 (2014).
2. Z. Du, T. D. Hatchard, R. A. Dunlap, and M. N. Obrovac, *J. Electrochem. Soc.*, **162**, A1858 (2015).
3. Z. Du, S. N. Ellis, R. A. Dunlap, and M. N. Obrovac, *J. Electrochem. Soc.*, **163**, A13 (2015).
4. Z. Du, T. D. Hatchard, P. Bissonnette, R. A. Dunlap, and M. N. Obrovac, *J. Electrochem. Soc.*, **163**, A2456 (2016).
5. Z. Du, R. A. Dunlap, and M. N. Obrovac, *J. Electrochem. Soc.*, **163**, A2011 (2016).
6. Z. Du, H. Liu, S. N. Ellis, R. A. Dunlap, M. Zhu, and M. N. Obrovac, *J. Electrochem. Soc.*, **163**, A1275 (2016).
7. H. Liu, M. Zhu, Z. Du, and M. N. Obrovac, *J. Electrochem. Soc.*, **163**, A192 (2015).
8. R. Beyers and R. Sinclair, *J. Appl. Phys.*, **57**, 5240 (1985).
9. Y. S. Lee, J. H. Lee, Y. W. Kim, Y. K. Sun, and S. M. Lee, *Electrochim. Acta*, **52**, 1523 (2006).
10. S. Zhou, X. Liu, and D. Wang, *Nano Lett.*, **10**, 860 (2010).
11. O. Park, J. -I. Lee, M. -J. Chun, J. -T. Yeon, S. Yoo, S. Choi, N. -S. Choi, and S. Park, *RSC Adv.*, **3**, 2538 (2013).
12. T. D. Hatchard, A. Genkin, and M. N. Obrovac, *AIP Adv.*, **7**, 45201 (2017).
13. Z. H. Yan, M. Oehring, and R. Bormann, *J. Appl. Phys.*, **72**, 2478 (1992).
14. M. N. Obrovac and L. J. Krause, *J. Electrochem. Soc.*, **154**, A103 (2007).
15. A. J. Smith, J. C. Burns, X. Zhao, D. Xiong, and J. R. Dahn, *J. Electrochem. Soc.*, **158**, A447 (2011).